Monthly Notices
of the
ROYAL ASTRONOMICAL SOCIETY

Mon. Not. R. Astron. Soc. **415,** 301–305 (2011) doi:10.1111/j.1365-2966.2011.18710.x

Suzaku observations of ejecta-dominated Galactic supernova remnant G346.6−0.2

A. Sezer,[1,2⋆] F. Gök,[3⋆] M. Hudaverdi,[1⋆] M. Kimura[4⋆] and E. N. Ercan[2⋆]

[1]*TÜBİTAK Space Technologies Research Institute, ODTU Campus, Ankara 06531, Turkey*
[2]*Boğaziçi University, Faculty of Art and Sciences, Department of Physics, Istanbul 34342, Turkey*
[3]*Akdeniz University, Faculty of Sciences, Department of Physics, Antalya 07058, Turkey*
[4]*Osaka University, Department of Earth and Space Science, Graduate School of Science, Machikaneyama 1-1, Toyonaka, Osaka 560-0043, Japan*

Accepted 2011 March 11. Received 2011 February 14; in original form 2010 December 15

ABSTRACT

We present here the results of an X-ray analysis of Galactic supernova remnant G346.6−0.2 observed with *Suzaku*. K-shell emission lines of Mg, Si, S, Ca and Fe are detected clearly for the first time. Strong emission lines of Si and S imply that the X-ray emission nature of G346.6−0.2 is ejecta-dominated. The ejecta-dominated emission is well fitted by a combined model consisting of a thermal plasma in non-equilibrium ionization and a non-thermal component, which can be regarded as synchrotron emission with a photon index of $\Gamma \sim 0.6$. An absorbing column density of $N_{\rm H} \sim 2.1 \times 10^{22}\,{\rm cm}^{-2}$ is obtained from the best fit, implying a high-density medium, high electron temperature of $kT_{\rm e} \sim 1.2$ keV and ionization time-scale of $n_{\rm e}t \sim 2.9 \times 10^{11}\,{\rm cm}^{-3}\,{\rm s}$, indicating that this remnant may be far from full ionization equilibrium. The relative abundances from the ejecta show that the remnant originates from a Type Ia supernova explosion.

Key words: ISM: individual objects: G346.6−0.2 – ISM: supernova remnants – X-rays: ISM.

1 INTRODUCTION

A supernova remnant (SNR) consists of expelled material called 'ejecta' from the explosion and swept-up interstellar matter. X-ray emission results from the interaction of ejecta and swept-up matter. From the X-ray emission of SNRs we may obtain valuable information about the physical properties of the ejecta, swept-up plasma, elemental abundances and history of the explosion. The shock wave may be the blast wave associated with the stellar explosion and/or the reverse shock wave, which propagates inwards from the decelerated blast wave and raises the temperature of the stellar ejecta. Young SNRs are bright in X-rays and dominated by emission from the ejecta. Thus they provide fruitful information about the elements synthesized by supernova (SN) explosions. Therefore, the observation of young SNRs is the best method by which to investigate the abundances of elements synthesized by SNe (see e.g. SN1006 (Koyama et al. 1995), RCW86 (Bamba, Koyama & Tomida 2000) and Tycho (Warren et al. 2005) for the best-studied ejecta-dominated SNRs in the X-ray band).

G346.6−0.2 (RA (2000) $= 17^{\rm h}10^{\rm m}19^{\rm s}$, Dec. (2000) $= -40^{\circ}11'$) is a shell-type SNR located in the Galactic plane. It was discovered by Clark, Caswell & Green (1975) in the radio band, with an angular size of 8 arcmin (Whiteoak & Green 1996). In the X-ray band, on the other hand, G346.6−0.2 was first observed by *ASCA* during its Galactic plane survey (Yamauchi et al. 2008). It is shown that the size of the X-ray emission from G346.6−0.2 is less extended than its reported radio structure. Five OH (1720-MHz) masers were detected toward this SNR and they are all located along the southern edge of the remnant (Koralesky et al. 1998).

We study the X-ray emission from ejecta-dominated SNRs. For this purpose we have chosen several small-size Galactic SNRs, one of which is G346.6−0.2. The detailed properties of G346.6−0.2 have remained unknown so far because of very limited photon statistics in the *ASCA* (*AGPS*) data. *Suzaku* is the most recent X-ray astronomical satellite (see Mitsuda et al. 2007), with a large collecting area and low background. Therefore, it is the best instrument for observing dim and diffuse sources. We propose here to study G346.6−0.2 in order to understand the origin of its thermal and non-thermal X-ray emission, which will help us to distinguish its SN explosion type. By using the archival data of *Suzaku*, we were able to produce a higher quality image and the spectra of the remnant, which lead to the results in this study.

In Section 2, we describe the observation log and the data-reduction methods. We present the image analysis in Section 2.1 and the spectral analysis in Section 2.2. We discuss our results and the origin of the thermal and non-thermal emission in Section 3.

⋆E-mail: aytap.sezer@uzay.tubitak.gov.tr (AS); gok@akdeniz.edu.tr (FG); murat.hudaverdi@uzay.tubitak.gov.tr (MH); mkimura@ess.sci.osaka-u.ac.jp (MK); ercan@boun.edu.tr (ENE)

2 OBSERVATIONS AND DATA REDUCTION

The *Suzaku* satellite has two sets of instruments, one being the four X-ray imaging spectrometers (XISs, see Koyama et al. 2007), each of these being at the focus of an X-ray telescope (XRT, see Serlemitsos et al. 2007), and also a separate hard X-ray detector (HXD, see Takahashi et al. 2007; Kokubun et al. 2007). XISs have two different types of CCD: one type consists of three front-illuminated CCDs (namely FI, XIS0, XIS2 and XIS3) and the other of a back-illuminated CCD (namely BI, XIS1). Each CCD covers an area of $17.8 \times 17.8\,\mathrm{arcmin}^2$.

The data used in this analysis are taken by the XIS on board *Suzaku*. G346.6−0.2 was observed on 2009 October 7 for 56.7 ks (Obs ID: 504096010). During the observation, the XISs were operated in the normal full-frame clocking mode with the editing mode of 3×3 and 5×5, which corresponds to low and medium data rates, high and superhigh data rates, respectively.

For the data reduction and spectral analysis, we used the HEADAS software package version 6.5 and XSPEC version 11.3.2 (see Arnaud 1996). The response matrix files (RMF) and ancillary response files (ARF) were made using XISRMFGEN and XISSIMARFGEN version 2006-10-17 (see Ishisaki et al. 2007).

2.1 Image analysis

Fig. 1 shows the XIS0 image of G346.6−0.2 in the 0.3–10 keV energy band. The solid circle (radius ∼5 arcmin) from the centre shows the region where the spectra are extracted. The background region is shown by a dotted circle (RA(2000) = $17^{\mathrm{h}}10^{\mathrm{m}}54^{\mathrm{s}}$, Dec. (2000) = $-40^{\circ}06'24''$, radius ∼1.8 arcmin). We excluded the upper right corner of the detectors containing the on-board masked-out ^{55}Fe calibration sources. For comparison, a radio continuum image of G346.6−0.2 at 843 MHz by Whiteoak & Green (1996) is overlaid on the figure, where four maser sources are also pointed out, as reported by Koralesky et al. (1998).

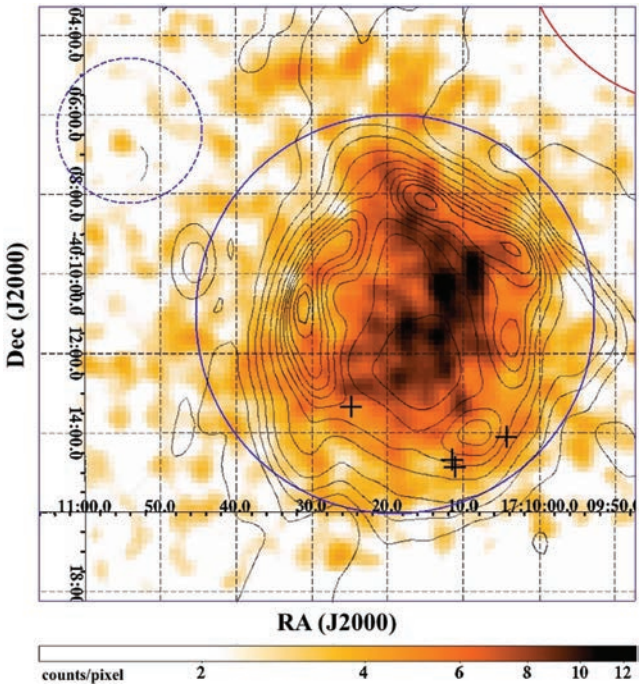

Figure 1. XIS0 image of G346.6−0.2 in the 0.3–10 keV full energy band. The coordinates are with reference to epoch J2000. The calibration source located at the upper right corner, as shown by a (red) circle, is masked out. The colour-coding is for X-ray photons in count pixel^{-1}. The overlaid isointensity contours are from radio observations at 843 MHz. The contour levels are −7, 6, 25, 50, 95, 135, 165, 190, 210, 230, 255 and 270 mJy beam^{-1}, selected to be the same as the radio work for visual comparison. The regions used to extract the spectrum and to determine the background parameters are indicated by blue solid and dotted circles, respectively. The positions of the four masers defined by Koralesky et al. (1998) are marked as crosses. (See the online article for the colour version of this figure.)

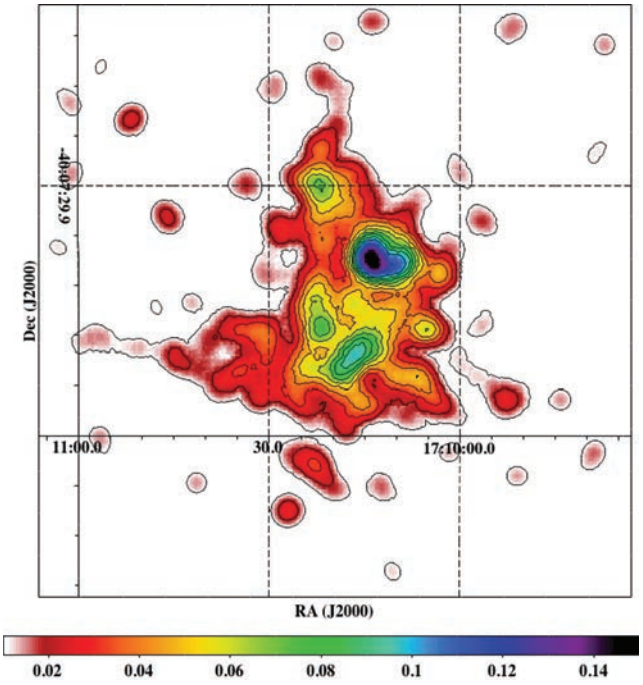

Figure 2. G346.6−0.2 XIS0 image in the 1.5–2.5 keV (Si–S) energy band. The image is smoothed for a 10σ Gaussian in order to highlight the Si–S distribution. Overlaid contours are spaced linearly in intensity (0.01, 0.02, 0.03, 0.05, 0.09 and 0.16 count pixel^{-1}). (see the online article for the colour version of the Figure.)

The bright image in XIS0 is clearly seen and we have obtained the Si–S map in the 1.5–2.5 keV energy band (Fig. 2) to see if this emission is from the interstellar medium (ISM) or the ejecta. In Fig. 2, the Si–S emission is distributed throughout the remnant and it is bright, which may well indicate that the X-ray emission coming from the remnant is ejecta-dominated rather than originating from the ISM.

2.2 Spectral analysis

The extracted XIS spectra from a circular region of G346.6−0.2 (see Fig. 1) are analysed in the full energy band of 0.3–10 keV. Fig. 3 shows representative spectra of XIS0, XIS1 and XIS3 simultaneously, extracted from the region shown in Fig. 1 by the solid circle, with its corresponding best-fitting model and residuals.

The strong Si and S lines from the spectra and Si–S image (see Fig. 2) in the 1.5–2.5 keV energy band suggest that the emission is ejecta-dominated. Therefore, we have applied one-component models in our spectral fits. We first fitted the data with an absorbed (wabs in XSPEC; Morrison & McCammon 1983) VNEI, which is a model for a non-equilibrium ionization (NEI) collisional plasma with variable abundances (Borkowski, Lyerly & Reynolds 2001). The model did not fit well (reduced χ^2 of 1.12; 637/567 degrees of freedom (d.o.f.)). We therefore added a power-law model (non-thermal synchrotron emission

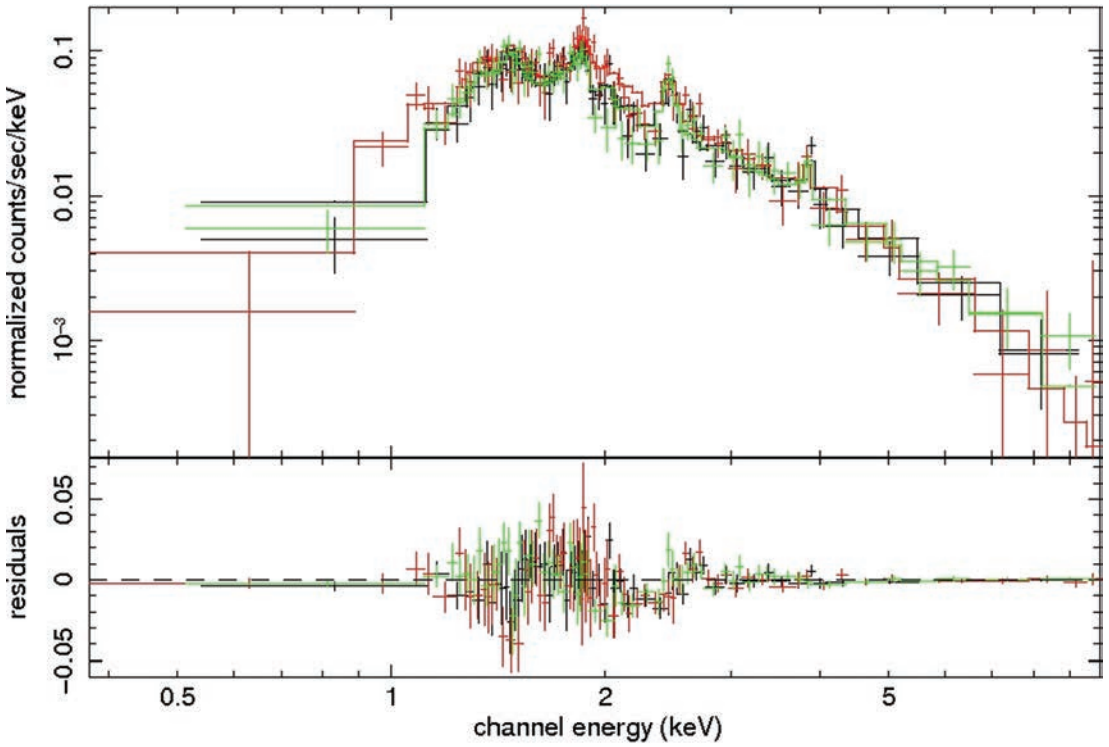

Figure 3. Background-subtracted XIS (XIS0: black, XIS1: red, XIS3: green) spectra of G346.6−0.2 in the full energy band (0.3–10 keV) fitted with an absorbed VNEI and power-law model. The lower panel shows the residuals from the best-fitting model. (See the online article for the colour version of this figure.)

from relativistic electrons). The parameters of the absorbing column density ($N_{\rm H}$), electron temperature ($kT_{\rm e}$), ionization parameter ($n_{\rm e}t$) and metal abundances C, N, O, Ne, Mg, Si, S, Ar, Ca and Fe are set free in this fit, resulting in an unacceptable error value. We then set Mg, S, Si, Ca and Fe free, since their emission lines are clearly seen in the spectra, while the rest are set to solar values (Anders & Grevesse 1989), resulting in a reasonably good reduced χ^2 value of 1.07 (606/565 d.o.f.) with reasonable error limits. Similar steps were also applied to the VMEKAL model in XSPEC, which describes an emission spectrum from hot ionized gas in collisional ionization equilibrium with variable abundances (Mewe, Gronenschild & van den Oord 1985; Mewe, Lemen & van den Oord 1986; Liedahl, Osterheld & Goldstein 1995), and the VPSHOCK model in XSPEC, which is suitable for modelling plane-parallel shocks in young SNRs where the plasma has not reached ionization equilibrium (Borkowski et al. 2001). These two models gave us reduced χ^2 values of 1.22 (691/568 d.o.f.) and 1.11 (629/567 d.o.f.), respectively. We then added a power-law component to both models, which yielded rather similar results (reduced χ^2/d.o.f. value of 607/566 and 605/565, respectively, for the best-fitting parameters and error values) to the VNEI model, as given in Table 1.

These three models basically represent the emission from an optically thin thermal plasma with slight differences. For example, VNEI is a NEI model similar to VPSHOCK, except with a single ionization time-scale.

From an absorbed VNEI and power-law model, the absorbing column density, electron temperature, ionization parameter, metal abundances of Mg, Si, S, Ca and Fe, volume emission measure (VEM) and flux ($F_{\rm x}$) of the VNEI component and photon index (Γ) and norm of the power-law component are obtained and are given in Table 1, together with the corresponding error values with 90 per cent confidence levels. The total flux and reduced χ^2/d.o.f. value of VNEI and power-law components are also given in this table. The results of VMEKAL and power-law, VPSHOCK and power-law models are also presented in Table 1 for comparison.

To determine the line-centre energy of the K-shell (Kα) lines, we fitted the spectra using a simple bremsstrahlung continuum plus five Gaussian lines with an absorbing column. The best-fitting central energies of Kα emission lines obtained are He-like Mg (1.38 ± 0.06 keV), Si (1.86 ± 0.02 keV), S (2.52 ± 0.06 keV), Ca (3.25 ± 0.55 keV) and Fe (6.77 ± 0.32 keV).

Fig. 4 shows the best-fitting metal abundances (normalized to Si) relative to solar values (Anders & Grevesse 1989) with the predicted nucleosynthesis W7 Type Ia SN model (Nomoto et al. 1997), which is widely used as the standard model.

3 DISCUSSION AND CONCLUSIONS

In this work, we provide for the first time a high-quality image, spectra and detailed description of the X-ray emission of G346.6−0.2 using a set of public archival *Suzaku* data. The radio emission of this remnant extends to 8 arcmin (Whiteoak & Green 1996), while the X-ray image shows a smaller extension (see Fig. 1) which is consistent with that of the *ASCA* results shown in Yamauchi et al. (2008).

We fitted the spectra with a 'thermal' component in non-equilibrium ionization and an additional 'non-thermal' power-law component with reasonably good χ^2 values.

3.1 Thermal emission

The thermal part of the spectra can be represented by a non-equilibrium ionization (VNEI) model. The thermal X-ray emission of young SNRs, emission from which is still dominated by ejecta, is predominantly from the ejecta heated by the reverse shock. Since

Table 1. The best-fitting parameters of the G346.6−0.2 spectra in the 0.3–10 keV energy band for VNEI, VMEKAL and VPSHOCK models.

Parameters	VNEI+power-law	VMEKAL+power-law	VPSHOCK+power-law
$N_{\rm H}$ ($\times 10^{22}$ cm^{-2})	2.1 ± 0.2	2.0 ± 0.2	2.1 ± 0.2
$kT_{\rm e}$ (keV)	1.22 ± 0.04	0.97 ± 0.05	1.3 ± 0.1
$n_{\rm e}t$ ($\times 10^{11}$ cm^{-3} s)	2.92 ± 0.01	–	$(6.92 \pm 0.01)^a$
Mg	0.51 ± 0.12	0.65 ± 0.15	0.76 ± 0.16
Si	0.47 ± 0.07	0.44 ± 0.07	0.56 ± 0.09
S	0.7 ± 0.1	0.7 ± 0.1	0.8 ± 0.1
Ca	2.3 ± 0.6	3.4 ± 0.8	2.3 ± 0.7
Fe	0.6 ± 0.3	0.4 ± 0.2	0.6 ± 0.3
VEM^b	11.6 ± 1.1	15.1 ± 1.9	10.4 ± 1.5
Flux^c	3.1 ± 0.5	2.9 ± 0.6	3.2 ± 0.4
Photon index	0.6 ± 0.3	0.5 ± 0.3	0.6 ± 0.3
norm ($\times 10^{-4}$ photon cm^{-2} s^{-1})	4.46 ± 0.04	4.55 ± 0.04	4.55 ± 0.05
Flux^d	4.4 ± 0.2	4.5 ± 0.2	4.4 ± 0.2
χ^2/d.o.f.	606/565 = 1.07	607/566 = 1.07	605/565 = 1.07

[a]The VPSHOCK fitting gives an upper limit on the ionization time-scale.
[b]Volume emission measure (VEM $= \int n_{\rm e} n_{\rm H}\, {\rm d}V$) in units of 10^{58} cm^{-3}, where $n_{\rm e}$ and $n_{\rm H}$ are number densities of electrons and protons, respectively and V is the X-ray-emitting volume.
[c]Flux in the 0.3–10 keV band in units of 10^{-11} erg s^{-1} cm^{-2}.
[d]Total flux in the 0.3–10 keV band in units of 10^{-11} erg s^{-1} cm^{-2}.

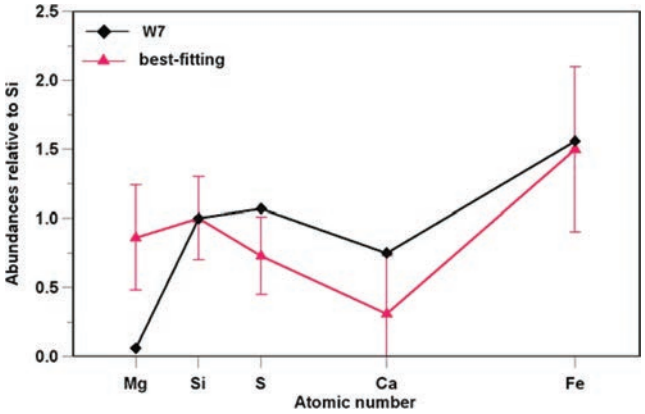

Figure 4. Metal abundances of Mg, S, Ca and Fe relative to solar values and normalized to Si. The W7 model for a Type Ia is shown by diamonds, while our data are shown by triangles.

the ejecta is metal-abundant, its X-ray spectra usually shows strong emission lines of heavy elements such as O, Ne, Mg, Si, S, Ar, Ca and Fe. Kα emission lines of Mg, Si, S, Ca and Fe for G346.6−0.2 are detected clearly for the first time in this work.

The interstellar absorbing column density $N_{\rm H}$ is found to be $(2.1 \pm 0.2) \times 10^{22}$ cm^{-2}, which is consistent with the Galactic value of $(1.5 \pm 0.2) \times 10^{22}$ cm^{-2} in that direction (Dickey & Lockman 1990). *ASCA* results of G346.6−0.2 reported a value of $N_{\rm H} > 10^{22}$ cm^{-2} (Yamauchi et al. 2008), indicating that the X-ray spectra of the remnant are heavily absorbed by interstellar matter, perhaps due to its location close to the Galactic plane. In other words, the electron density ($n_{\rm e}$) of the medium of the remnant is high enough. This may also be supported by the fact that the south region of the remnant is in interaction with four molecular clouds, as has been noted by Koralesky et al. (1998).

As the remnant is close to the Galactic plane and in a highly dense region, one can expect that some portions could be highly asymmetrical. The asymmetry in the south region of the remnant may well be due to interaction with maser sources, as has been noted in Fig. 1. One can argue that the surface brightness of the remnant is far from an equal distribution and spherical symmetry, due to the inhomogeneity of the medium.

The thermal emission further provides us with information about the electron temperature and age of the plasma. Our best-fitting temperature is obtained to be ∼1.2 keV, which is typical for shell-like SNRs. This value is also consistent with the result of ∼1.6 keV obtained from *ASCA* observations (Yamauchi et al. 2008).

The age of G346.6−0.2 has not been predicted so far. Of note is the fact that young SNRs with ages of a few hundred or about a thousand years are not only bright but also dominated by the emission from the ejecta. G346.6−0.2 is an ejecta-dominant remnant and bright in X-rays, and therefore could be a young SNR. The plasma in most young SNRs is in the NEI condition. The ionization age (or ionization parameter) is defined as $\tau = n_{\rm e}t$, which is often used as a key diagnostic of the NEI state. τ is typically required to be $\geq 10^{12}$ cm^{-3} s (Masai 1984) for full ionization equilibrium. In our observations we obtained a $n_{\rm e}t$ value of $(2.92 \pm 0.01) \times 10^{11}$ cm^{-3} s, which may also indicate that this SNR is far from full ionization equilibrium. Thus, the plasma has not yet had time to reach ionization equilibrium and is still being ionized. We calculated $n_{\rm e}$ to be ∼0.82 cm^{-3} from VEM $= n_{\rm e} n_{\rm H} V$, where $n_{\rm e} = 1.2 n_{\rm H}$ and V is the X-ray-emitting volume of the remnant (estimated to be $\sim 2 \times 10^{54}$ cm^3), by adopting an average distance of $d \sim 8.3$ kpc (the average of a near value of 5.5 kpc and far value of 11 kpc given by Koralesky et al. 1998) and assuming the emitting volume to be a spherical shell. From the equation $t = \tau / n_{\rm e}$, the age of G346.6−0.2 is calculated to be ∼1.1×10^4 yr. Thus, this remnant is likely to be the oldest known ejecta-dominated shell-like SNR (compared with SN1006, RCW86, G337.2-0.7 and G309.2-0.6 at ∼1000 (Yamaguchi et al. 2008a), ∼1800 (Yamaguchi et al. 2008b), 2000–4500 and 700–4000 yr (Rakowski, Hughes & Slane 2001), respectively).

3.2 Non-thermal emission

Recently, in some SNRs (e.g. first SN1006 (Koyama et al. 1995) and then RX J1713.7.3946 (Koyama et al. 1997; Slane et al. 1999), Cas A (Hughes et al. 2000; Vink et al. 2000) and Tycho's SNR (Hwang et al. 2002)) non-thermal emission has been detected. There are

two possible mechanisms for non-thermal emission: one is synchrotron emission and the other is non-thermal bremsstrahlung. The non-thermal emission coming from G346.6−0.2 is most likely synchrotron emission (power-law component with photon index of $\Gamma \sim 0.6$). The real source of synchrotron emission in SNRs is believed to be the acceleration of ultrarelativistic electrons in magnetic fields with the help of shock waves. A powerful X-ray point source inside the remnant or in the vicinity of the remnant can also contribute to the non-thermal emission. The photon index we obtained ($\Gamma \sim 0.6$) is lower (harder) than those of typical shell-like SNRs. This forces us to presume that a pulsar-wind nebula (PWN) contribution is also possible, although a PWN has not been discovered so far in or in the vicinity of G346.6−0.2.

The flux value of G346.6−0.2 obtained is $F_{\rm x} \sim 4.4 \times 10^{-11}$ erg s^{-1} cm^{-2} for the 0.3–10 keV range, which is in good agreement with that found with *ASCA* (Yamauchi et al. 2008). Using this flux value for the source and also taking an X-ray angular size of ∼5 arcmin, its surface brightness in the 0.3–10 keV energy range is found to be $\Sigma \sim 1.8 \times 10^{-12}$ erg s^{-1} cm^{-2} arcmin^{-2}, which is higher than for many shell-like Galactic SNRs. Surface brightness mainly depends on the explosion energy and the density of the medium, but a PWN may also contribute to the surface brightness of the SNR. In this case, the high medium density and small size of the remnant may be the main reason for the high X-ray surface brightness of G346.6−0.2.

3.3 Relative abundances in the ejecta

Theoretical models predict that in core-collapse SN explosions low-*Z* elements like O, Ne and Mg are produced (Thielemann, Nomoto & Hashimoto 1996), while in Type Ia SNe (Nomoto et al. 1997) high-*Z* elements like Ar, Ca and Fe are mostly produced. Furthermore, Fe production in Type Ia SNe is far larger than that in core-collapse SNe (Nomoto et al. 1997; Iwamoto et al. 1999). The detection of Fe emission lines from remnants is important to identify the type of remnant. *Suzaku* has detected Fe Kα lines in Type Ia SNRs in particular (e.g. Tycho, SN1006, RCW86).

When we compare our best-fitting abundances of Mg, S, Ca and Fe relative to Si with the predicted theoretical values, Mg relative to Si is higher while S and Ca relative to Si are lower. The reason for the lower abundances of S and Ca could be that the elements are concentrated at the inner layers of the remnant and hence are not yet heated enough by the reverse shock. This information implies that this SNR is in its early evolution phase. Our best-fitting abundance of Fe relative to Si is consistent with the expected value (see Fig. 4) within the confidence range. However, considering the large error bars due to low statistics, we could also make a similar statement for the Fe abundance value and an unattained reverse shock, as is reported in many Type Ia SNRs like SN1006 (Yamaguchi et al. 2008a), Tycho (Tamagawa et al. 2009) and G337.2-0.7 (Rakowski et al. 2001), the Fe abundance being less than the expected value produced in a Type Ia SN. Considering all these cases, we can predict that the remnant may originate from a Type Ia SN explosion.

ACKNOWLEDGMENTS

AS is supported by a TÜBİTAK PostDoctoral Fellowship. This work is supported by the Akdeniz University Scientific Research Project Management and by TÜBİTAK under project codes 108T226 and 109T092. The authors also acknowledge support by the Boğaziçi University Research Foundation under 2010–Scientific Research Project Support (BAP) project no. 5052.

REFERENCES

Anders E., Grevesse N., 1989, Geochim. Cosmochim. Acta, 53, 197
Arnaud K. A., 1996, in Jacoby G., Barnes J., eds, ASP Conf. Ser. Vol. 101, Astronomical Data Analysis Software and Systems V. Astron. Soc. Pac., San Francisco, p. 17
Bamba A., Koyama K., Tomida H., 2000, PASJ, 52, 1157
Borkowski K. J., Lyerly W. J., Reynolds S. P., 2001, ApJ, 548, 820
Clark D. H., Caswell J. L., Green A. J., 1975, Australian J. Phys. Astrophys. Suppl., 37, 1
Dickey J. M., Lockman F. J., 1990, ARA&A, 28, 215
Hughes J. P., Rakowski C. E., Burrows D. N., Slane P. O., 2000, ApJ, 528, L109
Hwang U., Decourchelle A., Holt S. S., Petre R., 2002, ApJ, 581, 1101
Ishisaki Y. et al., 2007, PASJ, 59, 113
Iwamoto K., Brachwitz F., Nomoto K., Kishimoto N., Umeda H., Hix W. R., Thielemann F.-K., 1999, ApJS, 125, 439
Kokubun M. et al., 2007, PASJ, 59, 53
Koralesky B., Frail D. A., Goss W. M., Claussen M. J., Green A. J., 1998, AJ, 116, 1323
Koyama K., Petre R., Gotthelf E. V., Hwang U., Matsuura M., Ozaki M., Holt S. S., 1995, Nat, 378, 255
Koyama K., Kinugasa K., Matsuzaki K., Nishiuchi M., Sugizaki M., Torii K., Yamauchi S., Aschenbach B., 1997, PASJ, 49, L7
Koyama K. et al., 2007, PASJ, 59, 23
Liedahl D. A., Osterheld A. L., Goldstein W. H., 1995, ApJ, 438, L115
Masai K., 1984, Ap&SS, 98, 367
Mewe R., Gronenschild E. H. B. M., van den Oord G. H. J., 1985, A&AS, 62, 197
Mewe R., Lemen J. R., van den Oord G. H. J., 1986, A&AS, 65, 511
Mitsuda K. et al., 2007, PASJ, 59, 1
Morrison R., McCammon D., 1983, ApJ, 270, 119
Nomoto K., Iwamoto K., Nakasato N., Thielemann F.-K., Brachwitz F., Tsujimoto T., Kubo Y., Kishimoto N., 1997, Nucl. Phys. A, 621, 467
Rakowski C. E., Hughes J. P., Slane P., 2001, ApJ, 548, 258
Serlemitsos P. J. et al., 2007, PASJ, 59, 9
Slane P., Gaensler B. M., Dame T. M., Hughes J. P., Plucinsky P. P., Green A., 1999, ApJ, 525, 357
Takahashi T. et al., 2007, PASJ, 59, 35
Tamagawa T. et al., 2009, PASJ, 61, 167
Thielemann F-K., Nomoto K., Hashimoto M., 1996, ApJ, 460, 408
Vink J., Kaastra J. S., Bleeker J. A. M., Bloemen H., 2000, Adv. Space Res., 25, 689
Warren J. S. et al., 2005, ApJ, 634, 376
Whiteoak J. B. Z., Green A. J., 1996, A&AS, 118, 329
Yamaguchi H. et al., 2008a, PASJ, 60, 141
Yamaguchi H., Koyama K., Nakajima H., Bamba A., Yamazaki R., Vink J., Kawachi A., 2008b, PASJ, 60, 123
Yamauchi S., Ueno M., Koyama K., Bamba A., 2008, PASJ, 60, 1143

This paper has been typeset from a TEX/LATEX file prepared by the author.